Electronic Supplementary Material (ESI) for Journal of Materials Chemistry A.

Supporting Information

Formation Mechanism of Janus Nanostructures in One-Pot Reactions: The Case of Ag-Ag_8GeS_6

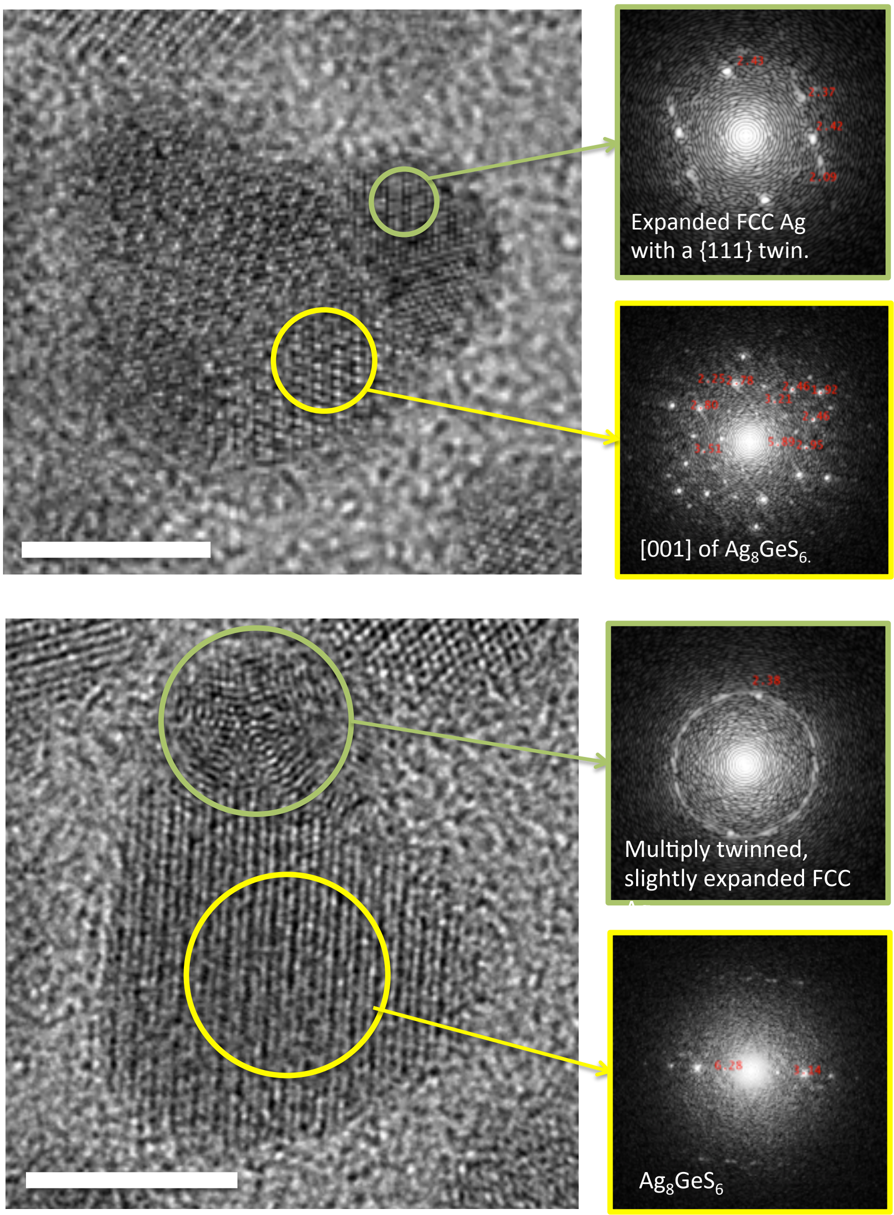

Figure S1: HRETM images and the corresponding FFT images of the final isolated Janus nanostructures. These images highlight the different morphologies of the Ag component found in a typical sample. The top panel shows an Ag-Ag_8GeS_6 nanostructure with a bulk Ag_8GeS_6 component and twinned FCC Ag component, which has a slightly expanded lattice parameter. The lower panel shows another image typical of the morphology of the Ag-Ag_8GeS_6 nanostructures, which dsiplays a penta-twined Ag component. Scale bars= 5nm.

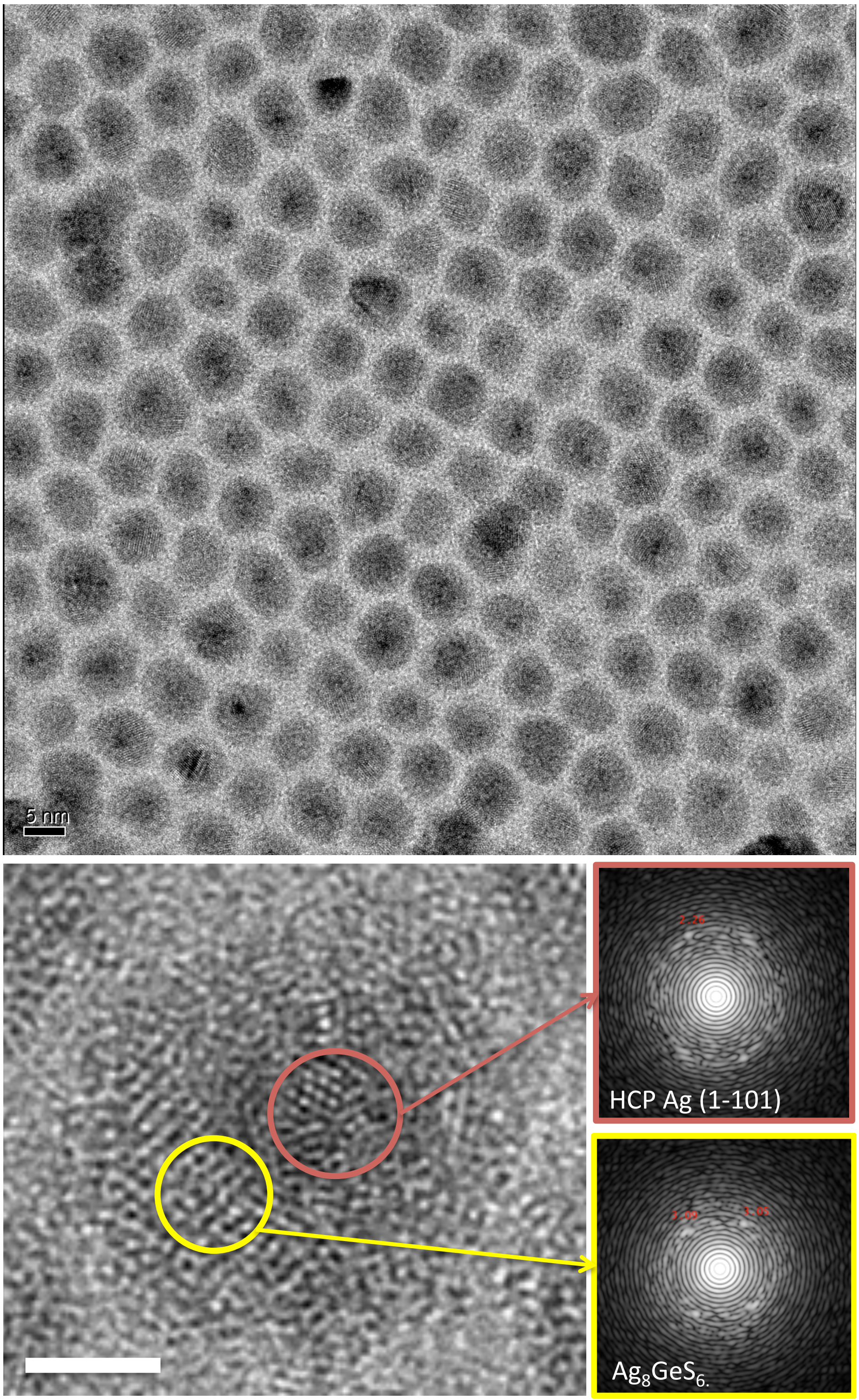

Figure S2: Top panel: HRETM image of the Ag/Ag_8GeS_6 core/shell nanocrystals. Lower panel: A single Ag/Ag_8GeS_6 nanocrystal and the corresponding FFT images that shows the crystal structure of both the core and the shell. In this case the Ag core may be indexed to [011] HCP Ag d(2.26Å). Scale bar of lower image, 2 nm.

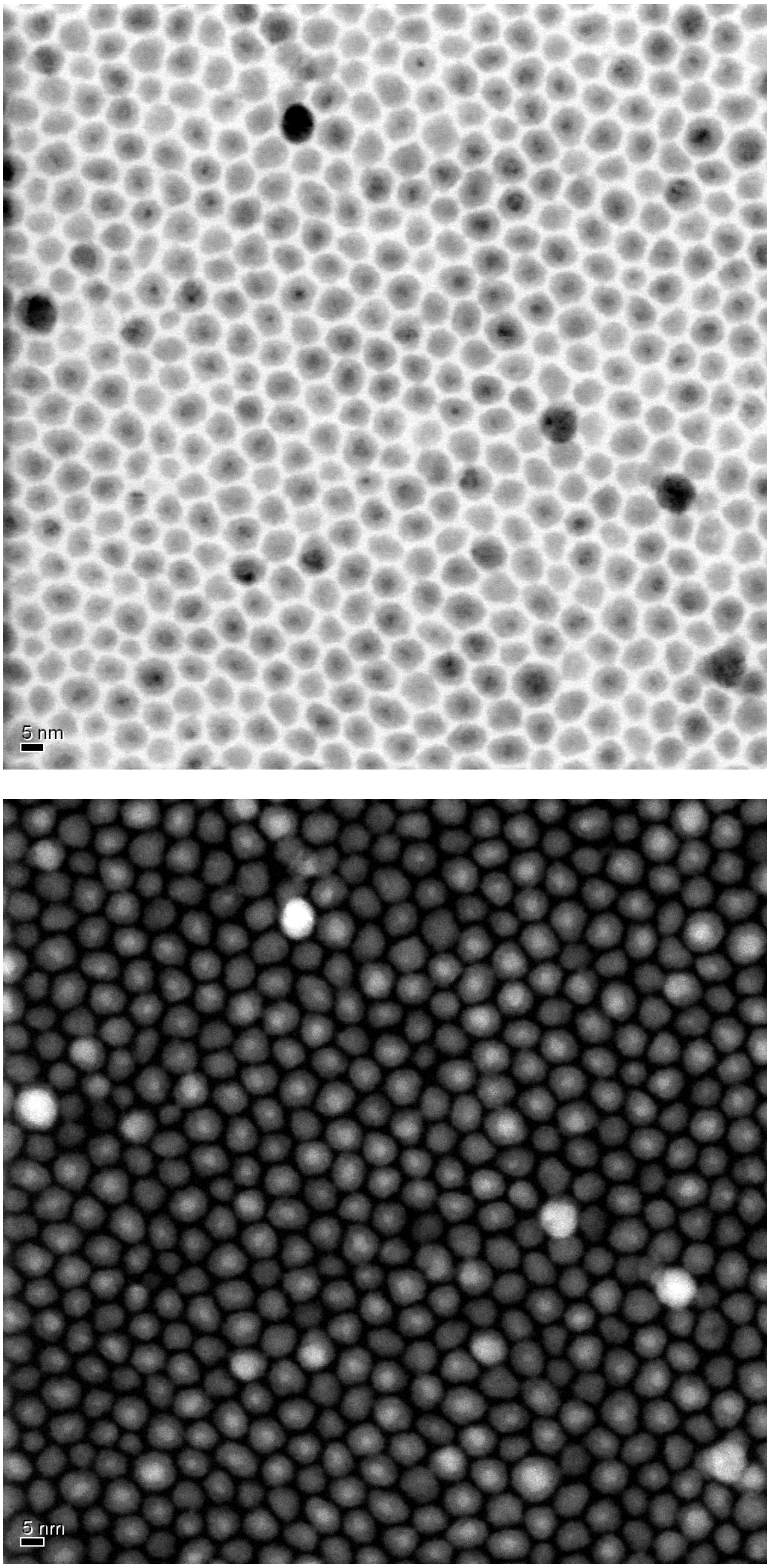

Figure S3: HRETM images in bright field (top panel) and dark field (lower panel) modes of a sample of Ag/Ag_8GeS_6 core/shell nanocrystals used to evaluate the mean core/shell size and the diameter of the Ag core.

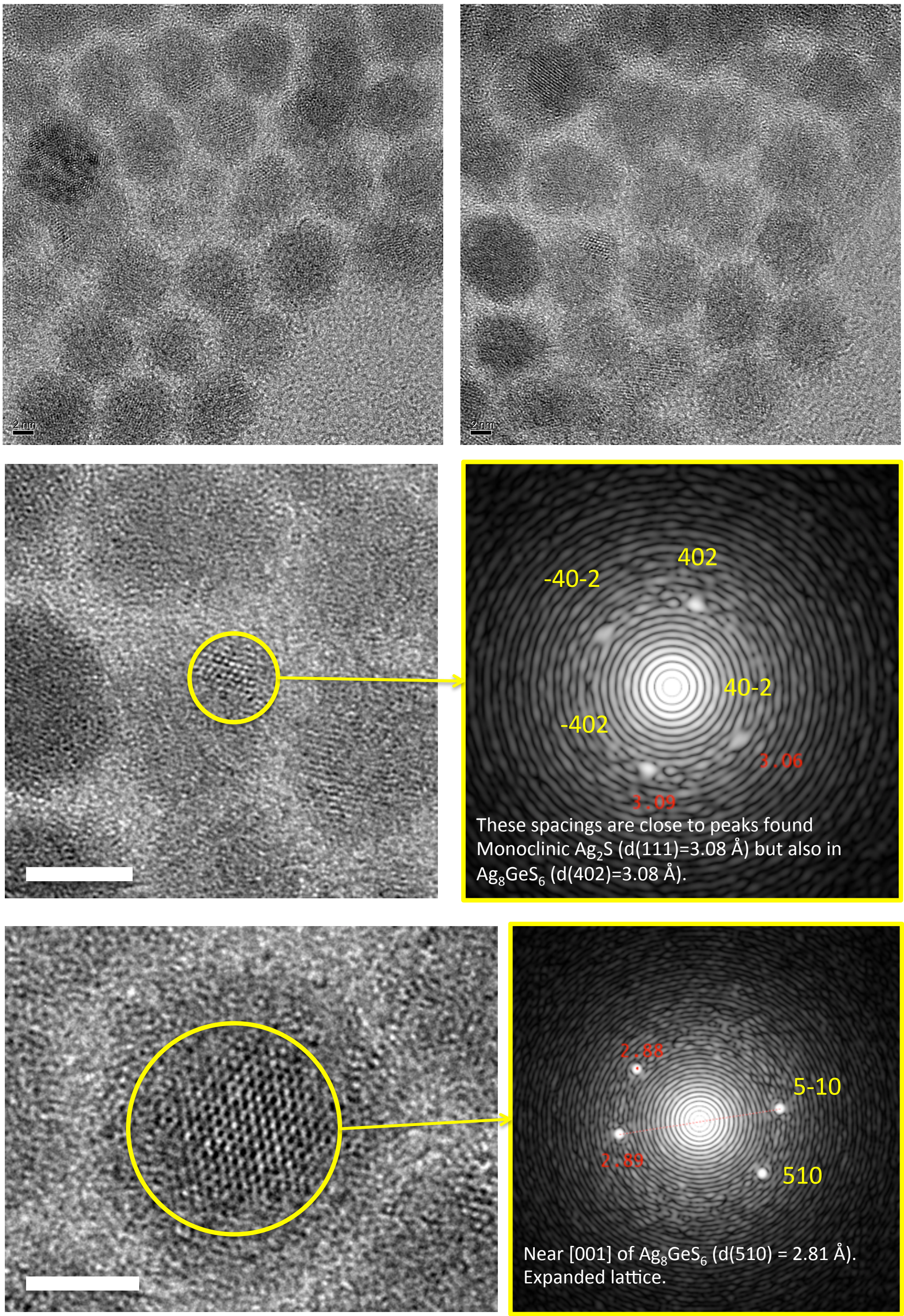

These spacings are close to peaks found Monoclinic Ag_2S (d(111)=3.08 Å) but also in Ag_8GeS_6 (d(402)=3.08 Å).

Near [001] of Ag_8GeS_6 (d(510) = 2.81 Å). Expanded lattice.

Figure S4: Top panel: HRTEM images of the initial nanoparticles isolated at 100 °C. A large number of the nanoparticles were devoid of obvious lattice fringes. However, some displayed patches of crystalline material, which could be indexed to either Ag_2S or Ag_8GeS_6 (middle panel) or Ag_8GeS_6 explicitly (lower panel). Scale bars of lower two panels = 5nm.

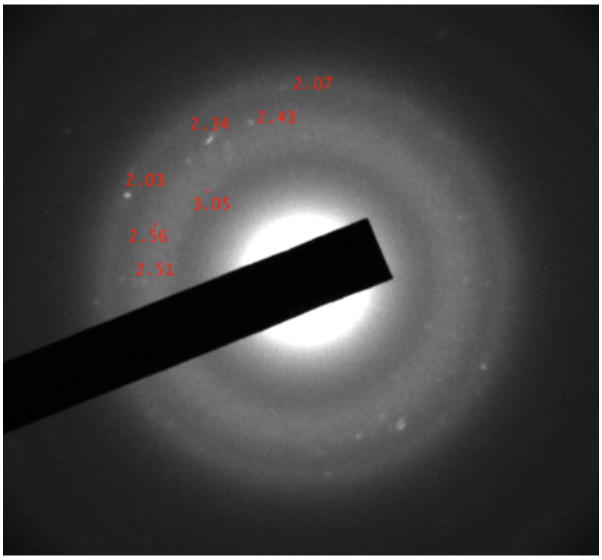

Figure S5: Electron diffraction pattern of the nanoparticles isolated at 100 °C. This pattern shows only a few spots over a diffuse background, implying that most of the material is amorphous or poorly crystalline. The spots are consistent with Ag_8GeS_6 (3.05 Å, ~2.56 Å, 2.07 Å), FCC Ag (2.03 Å, 2.34 Å), expanded FCC Ag-Ge (2.07 Å, 2.43 Å) and HCP Ag (2.51 Å).

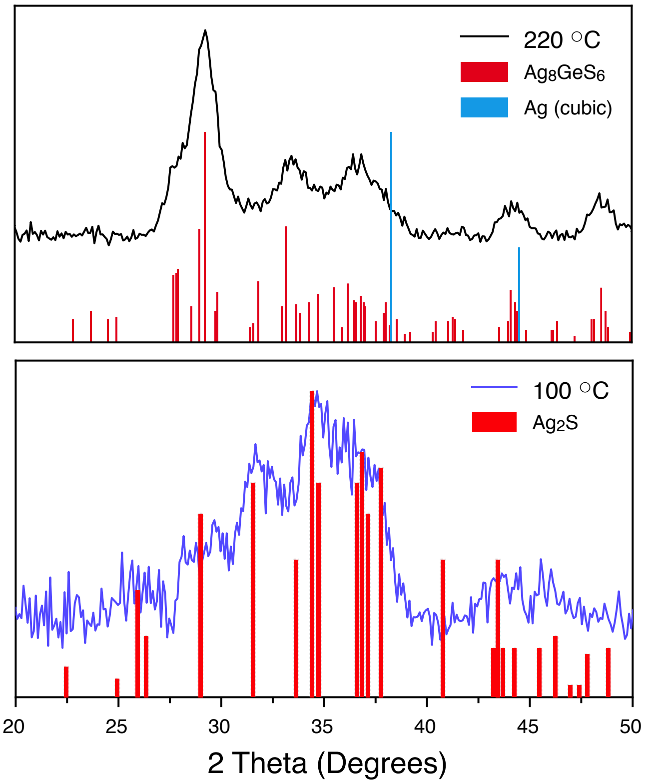

Figure S6: XRD pattern of the nanostructures isolated at 220 °C (top panel) and a magnified pattern of the nanoparticles isolated at 220 °C (lower panel). The nanoparticles isolated at low temperature are seen to have a low signal to noise ratio and very broad peaks consistent with poorly crystalline material. Nevertheless, the overall shape of the pattern and the relative peak intensities match quite well to monoclinic Ag_2S (ICCD #14-0072).

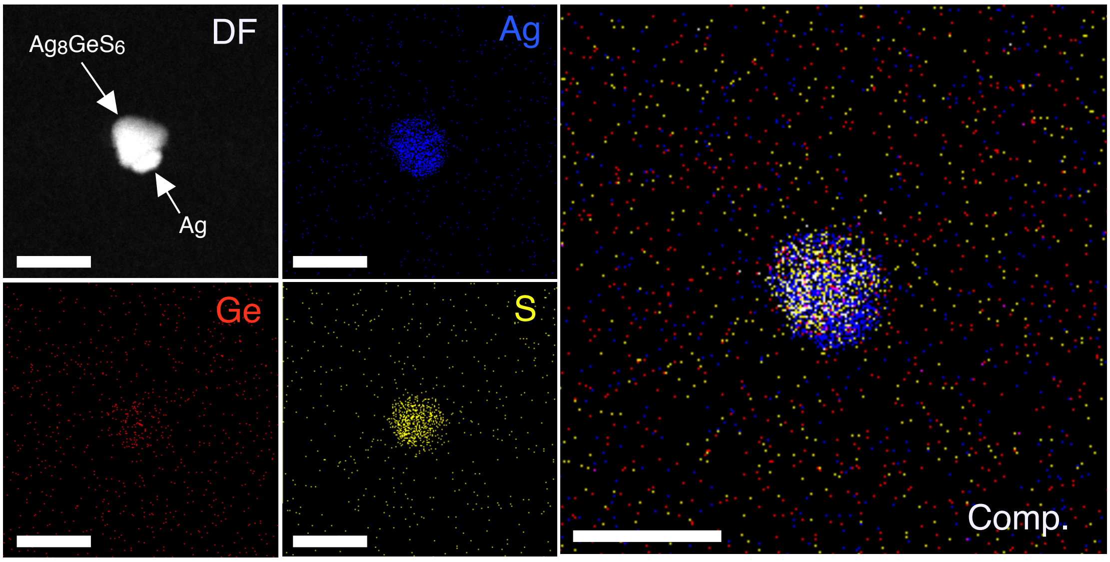

Figure S7: STEM-XEDS map of the final Janus nanostructure. The arrows in the DF image show the positions of the Ag_8GeS_6 (semiconductor) and Ag (metal components. The corresponding Ag (blue), Ge (red), S (yellow), and composite elemental maps are shown. From the elemental maps it can be clearly seen that silver spans the entire particle, while the sulfur is located to the semiconductor component. We note a very small signal (slightly above background) from sulfur in the region of the Ag component. As the semiconductor–metal interface might not be parallel to the electron beam it is impossible to determine if some residual signal is arising from an underlying semiconductor portion below the Ag component.

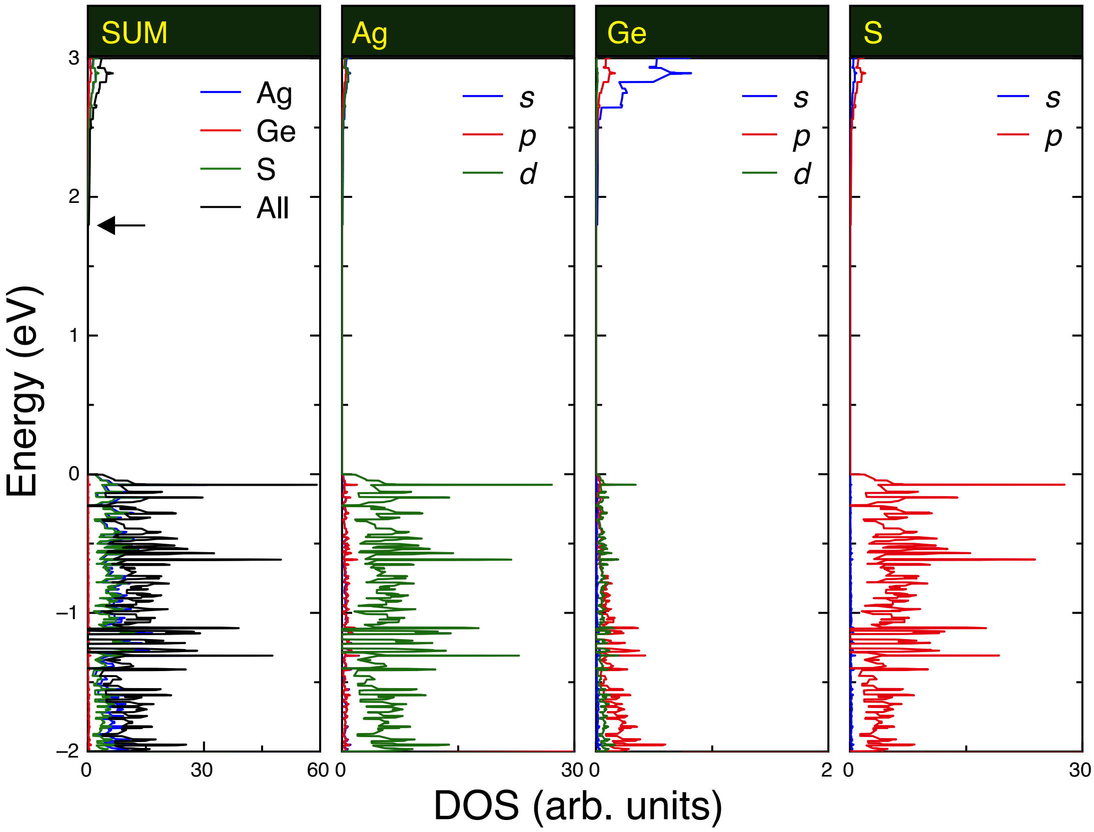

Figure S8: To gain a better understand the optoelectronic properties of the Janus nanostructures Ag-Ag_8GeS_6 system, the electronic structure of the semiconductor component was modeled using a generalize gradient approximation (GGA) and HSE06 functional, with the geometry optimized in the space group *Pna21*. GGA-PBE calculations show that Ag_8GeS_6 has a direct band gap at a Γ-point of 0.62 eV. As this value is lower than the experimentally determined band gap of ~1.4 eV, more accurate values were achieved by applying the HSE06 functional, which yielded a direct band gap of ~1.79eV (as indicated by the arrow).

From the total and partial density of states (DOS) of Ag_8GeS_6 we observe that large amount of states are around the upper valence band minimum and largely contributed by Ag 4*d* orbitals, while the lower conduction band is mainly comprised of S 2*p* orbitals and 5*s* orbitals from Ag. The states from Ge only account for a small fraction of the total DOS. However, their position close to the Fermi level significantly influences the band gap. The partial DOS revealed hybridization of states between Ag-*s,p*, Ge-*p,d* and S-*p* orbitals. As such, it is possible that additional states (at the metal-semiconductor interface) arising from Ag perturb the band gap and increase its experimentally calculated energy (at ~1.6 eV) relative to the known value for bulk Ag_8GeS_6 (~1.4 eV).